minerals

MDPI

Article

Genesis of the Triassic Polyhalite in the Quxian Area, Northeastern Sichuan Basin, China: Evidence from Sedimentary Characteristics and Evaporite Sulfur Isotope Geochemistry

Fanfan Zuo [1], Yongsheng Zhang [1,2,3,*], Baoling Gui [1], Enyuan Xing [1], Kui Su [1] and Xinsheng Niu [1]

[1] MNR Key Laboratory of Saline Lake Resources and Environments, Institute of Mineral Resources, Chinese Academy of Geological Sciences, Beijing 100037, China; fanfan.zuo@hotmail.com (F.Z.); guizi0603@163.com (B.G.); xingenyuan2022@126.com (E.X.); ssskkk@126.com (K.S.); xsh_niu@foxmail.com (X.N.)
[2] MNR Key Laboratory of Metallogeny and Mineral Assessment, Institute of Mineral Resources, Chinese Academy of Geological Sciences, Beijing 100037, China
[3] State Key Laboratory of Deep Earth and Mineral Exploration, Institute of Mineral Resources, Chinese Academy of Geological Sciences, Beijing 100037, China
* Correspondence: zys_601@126.com

Abstract

Shallow polyhalite potash ore hosted in the Lower–Middle Triassic evaporites of the Quxian area, northeastern Sichuan Basin, has been known since the 1980s. The uncertainty regarding its genesis has hindered the exploration of marine potash deposits in the study area and elsewhere worldwide. Sedimentological and sulfur isotope analyses of the newly drilled well LJ1 core were carried out. Four microfabric types of polyhalite (PM1–PM4) are recognized within four types of polyhalite rock. Their $\delta^{34}S$ values average 29.7 ‰, consistent with globally high Early Triassic values and indicating a ^{34}S-enriched seawater source. The microfabric types record multi-stage sedimentation and a genetic model of the study area polyhalite is established. Fine-grained polyhalite (PM1) represents primary or penecontemporaneous origin, formed by the K^+- and Mg^{2+}-rich brine supplied from the adjacent areas mixed with the Ca^{2+} and SO_4^{2-}-rich brine formed by in situ evaporation. Fibrous (PM2) and metasomatic relict-textured (PM4) polyhalite formed later at polyhalite–anhydrite contacts through metasomatism. Prismatic polyhalite (PM3) formed in both settings. The comparison of sulfur isotopes among different minerals and among evaporites from different regions provides important evidence for the sources of the ore-forming material and further verifies the above-mentioned genetic model.

Keywords: polyhalite; sulfur isotope; microfabrics; Lower–Middle Triassic; northeastern Sichuan Basin

Academic Editor: Davide Lenaz

Received: 17 October 2026
Revised: 11 November 2026
Accepted: 24 November 2026
Published: 25 November 2026

Copyright: © 2026 by the authors. Licensee MDPI, Basel, Switzerland. This article is an open access article distributed under the terms and conditions of the Creative Commons Attribution (CC BY) license.

1. Introduction

Polyhalite, with the ideal formula $K_2SO_4{\cdot}MgSO_4{\cdot}2CaSO_4{\cdot}2H_2O$, is a compound sulfate mineral rich in potassium, magnesium, calcium and sulfur. Unlike conventional soluble potash minerals such as sylvite and carnallite, polyhalite dissolves slowly. This makes it a naturally high-quality slow-release compound fertilizer enriched in sulfur, calcium, potas-

sium and magnesium. Polyhalite is a common constituent of many ancient evaporitic systems, particularly during the Permian–Triassic and Neogene [1–3]. In China, it is found mainly in the salt basins of the Sichuan Basin, the Qaidam Basin and the Jianghan Basin [4]. Among these, the Middle–Lower Triassic marine salt-bearing strata of the Sichuan Basin host the most widely distributed and potentially the largest polyhalite resources, with predicted prospective resources exceeding ten billion tonnes of K_2O in an early prediction [5].

Several salt-bearing formations developed within the thick carbonate–evaporite system of the Middle–Lower Triassic in the Sichuan Basin, and polyhalite-bearing strata have been discovered in several regions [4,6–8]. Research on the genesis of polyhalite in the basin began in the 1980s [9–16]. However, because polyhalite is widely distributed across the basin, its genetic categories and formation conditions may differ markedly from region to region, and its genesis remains debated. Early studies mostly favoured a metasomatic origin. More recent work, based on geochemical and textural observations, tends towards a penecontemporaneous or primary origin that may coexist with metasomatic overprints [13,15,17].

Hou et al. [18] compared the genesis of different polyhalite types mainly on the basis of microscopic observations. They concluded that polyhalite in paragenesis with halite precipitated primarily, whereas polyhalite associated with anhydrite is of metasomatic origin. The former interpretation has gained support in recent years from sedimentary evolution, Sr and S isotope data and other geochemical evidence. Its typical representative is the polyhalite in paragenetic with halite in the Xuanhan area of northeastern Sichuan, referred to as the "new type of polyhalite potash deposit" [8,19]. The results indicate that primary precipitation is the dominant process for halite-associated polyhalite, although a small amount of metasomatic polyhalite also developed owing to multi-stage overprinting. The polyhalite in the Quxian area is a typical representative of polyhalite in paragenesis with anhydrite. Compared with anhydrite-associated polyhalite in other regions, it is buried much shallower as a result of tectonic activities. Whereas polyhalite in most other areas lies at depths greater than 2000 m, that in the Quxian area is generally shallower than 1000 m, which is favourable for mining and utilization. Owing to factors such as complex geological structures, highly variable ore-layer thicknesses and an unclear distribution pattern, however, exploration and evaluation of the polyhalite potash in this area were carried out mainly during the 1980s and 1990s and then essentially stalled, and no consensus has been reached on its genetic mechanism.

In order to provide further evidence for the genetic mechanism of polyhalite in the Quxian area, this study uses core material from the newly drilled well LJ1 (Figure 1c). XRD analysis of evaporites in the ore interval, macroscopic observation of hand specimens, microscopic observation and sulfur isotope measurement are combined to determine the classification and genetic types of polyhalite in the study area. The results are then compared with data on polyhalite in the Xuanhan area, and the differences in the genesis of different polyhalite types across the Sichuan Basin are discussed. The results also help to identify the distribution characteristics and patterns of polyhalite, and thus offer new constraints for future potash exploration and development in this region and in similar evaporitic settings.

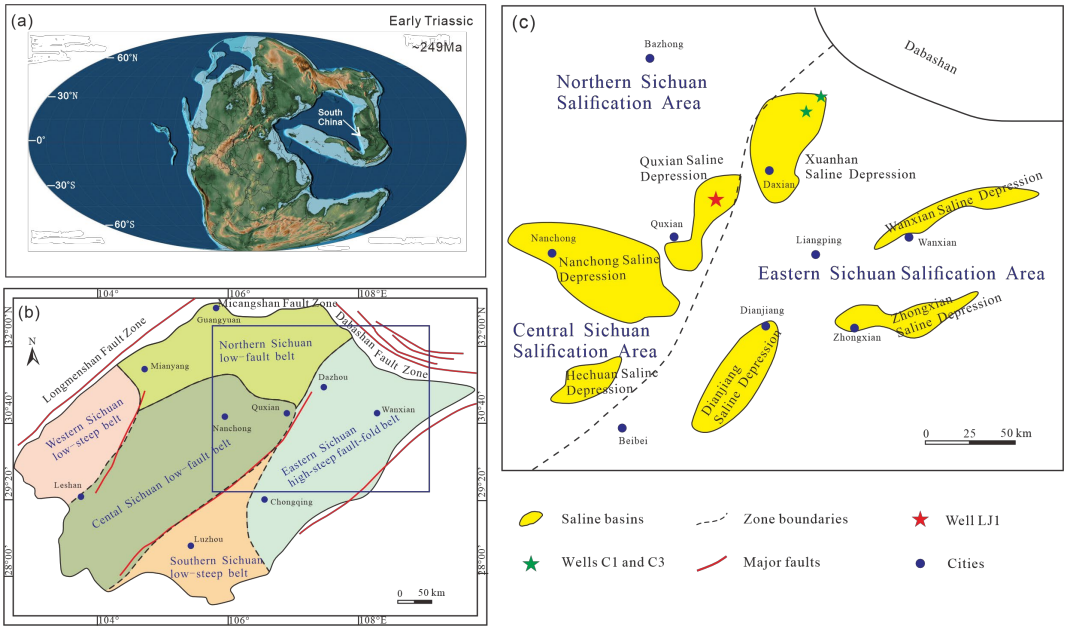


Figure 1. (**a**) Early Triassic plate tectonic maps by C.R. Scotese, PALEOMAP Project [20]; (**b**) Simplified regional geological map of the Sichuan Basin; (**c**) Distribution of salt basins in the study area and adjacent area (after reference [17]).

2. Geological Setting

The Sichuan Basin lies on the northwestern margin of the Upper Yangtze Block at the eastern edge of the Palaeo-Tethys Ocean and forms a rhombic tectonic–sedimentary unit bounded by intersecting NE- and NW-trending deep-seated faults (Figure 1a,b) [6,21]. Its sedimentary evolution was governed by multiple phases of tectonic activity [21]. After the Permian plate collision, the mountain ranges around the basin were progressively uplifted under the influence of the Indosinian Orogeny during the Early to Middle Triassic, and a series of platform-margin uplift belts formed. The Sichuan Basin was thus transformed from an open shelf into a restricted platform [6,22]. At the same time, the Luzhou–Kaijiang palaeo-uplift kept growing and blocked seawater intrusion from the southeast. This imposed strong sedimentary differentiation across the platform and produced relatively isolated depressions in northeastern Sichuan that were favourable for salt accumulation (Figure 1c) [21,23]. Within this tectonic framework, the marine evaporite–carbonate system of the basin evolved from carbonate-dominated to evaporite-dominated lithologies, and finally formed an evaporitic succession composed mainly of anhydrite and halite with interbedded polyhalite [21,23,24]. From the Middle to Late Triassic, the periphery of the Sichuan Basin changed from a passive continental margin into a foreland basin in response to the continental-collision phase of the Indosinian Orogeny. By the end of the Middle Triassic, marine sedimentation had ended and was replaced by continental deposition [22].

Under this tectonic and palaeoclimatic background, a hot and arid climate prevailed over the Yangtze Platform during the Early-Middle Triassic [25–27]. Several salt-forming episodes were recorded in the Lower–Middle Triassic evaporite–carbonate system of the Sichuan Basin, with anhydrite–salt layers locally reaching several hundred metres in thickness [7,12,28]. Among these, a light-green cemented clay bed (commonly referred to as “green-bean rock”) is widely distributed across the Yangtze Platform. It is an altered felsic volcanic ash (K-bentonite) and serves as an isochronous marker horizon for defining and correlating the Lower–Middle Triassic boundary (the top of the Jialingjiang Formation and the base of the Leikoupo Formation) [29,30]. Polyhalite is commonly found in two types of potassium-bearing sedimentary sequences. One is a sedimentary sequence associated with halite, in which polyhalite occurs mainly as discrete layers or as mixed

lumps with anhydrite. The polyhalite in the Xuanhan area of northeastern Sichuan belongs to this type. The other is a sedimentary sequence associated with anhydrite, in which no halite deposition is observed. The polyhalite in the studied Quxian area belongs to this latter type. The study area is located in Quxian, northeastern Sichuan Basin, and structurally occupies the core of the NE-trending Huayingshan anticline. The shallow polyhalite in the study area is hosted mainly within the Middle Triassic Leikoupo Formation, which records the most important salt-forming episodes of the Early–Middle Triassic in the Sichuan Basin.

3. Materials and Methods

Core samples were collected from well LJ1, which targets the Lower Triassic fourth and fifth members of the Jialingjiang Formation (T_1j^{4+5}) and the first member of the Middle Triassic Leikoupo Formation (T_2l^1) in the northeastern Sichuan Basin. A total of 320 m of core was examined and described macroscopically. Subsequently, 27 thin sections composed of polyhalite and/or anhydrite were analyzed in detail. All samples were carefully examined, described and photographed under a Leica DM2700P polarizing microscope (Leica Microsystems, Wetzlar, Germany).

Scanning electron microscopy (SEM) was performed on selected key thin sections at the MNR Key Laboratory of Metallogeny and Resource Assessment, Institute of Mineral Resources, Chinese Academy of Geological Sciences (IMR, CAGS), using a ZEISS Ultra Plus field-emission scanning rlectron microscope (Carl Zeiss AG, Oberkochen, Germany). Evaporitic minerals are unstable under electron beams, so an acceleration voltage of 15 kV was used to ensure analytical precision.

On the basis of the integrated sedimentological work described above, 81 fresh whole-rock samples were selected and ground to 200 mesh for geochemical analysis. The average sampling interval across the ore interval was 2.7 m, and sampling was intensified within polyhalite-rich horizons.

X-ray diffraction (XRD) analysis of these samples was carried out by the Beijing Beida Yanyuan Microstructure Analysis and Testing Centre for semi-quantitative analysis of the bulk rock. The analysis was performed on a D8 Advance powder diffractometer with a voltage of 40 kV, a current of 40 mA, a Cu target, a measurement range of 3–90°, an angular accuracy of ±0.0001° and a scanning rate of 8 °/min.

Sulfur isotope measurements were performed on the same 81 samples at the MNR Key Laboratory of Metallogeny and Resource Assessment, IMR, CAGS, using a Flash 2000-HT system. For each analysis, 300 μg of V_2O_5 was mixed with 100 μg of pure sulfate sample. The mixture was placed in a tin cup and introduced into the reactor. Oxygen was introduced at the same time, and the reaction furnace was set to 1020 °C. The sample and the tin cup burned rapidly, and the SO_2 produced was delivered to the mass spectrometer. The analysis was calibrated with the three international reference materials IAEA-SO-5, IAEA-SO-6 and NBS127. The results are reported relative to V-CDT, with an analytical precision better than 0.2 ‰.

In addition, the SO_4^{2-} contents of the whole-rock samples were determined by water-soluble chemical experiments at the Shandong Lunan Geological Engineering Survey Institute. The samples were ground to 200 mesh. One gram of each powder was added to 50 mL of distilled water, stirred thoroughly and left to stand for 12 h. After the solution had been made up to a constant volume of 100 mL, the SO_4^{2-} content was determined by the barium chloride gravimetric method.

4. Results

The polyhalite ore and the ore beds were studied by combining XRD data with hand-specimen observation of drill cores and microscopic identification of thin sections (Figure 2). Rock classification and description were carried out first, so that the mode of occurrence of the ore body, its lithological association, textures and structures, and paragenetic relationships could be established. Microscope observation then provided the microfabrics of the polyhalite minerals. Finally, the XRD data were used to divide the ore beds penetrated by the well. The polyhalite-bearing beds occur mainly between 142 and 365 m and can be divided into four ore beds from bottom to top (ore beds I, II, III and IV). Ore bed I consists of several thin ore layers separated by anhydrite layers. Apart from an ultra-thin polyhalite-bearing layer at its base, ore bed II is essentially continuous; its polyhalite content varies rhythmically, and its individual layers are the thickest among the four beds. Ore beds III and IV both consist of a thin layer at the base and medium- to thick layers above.

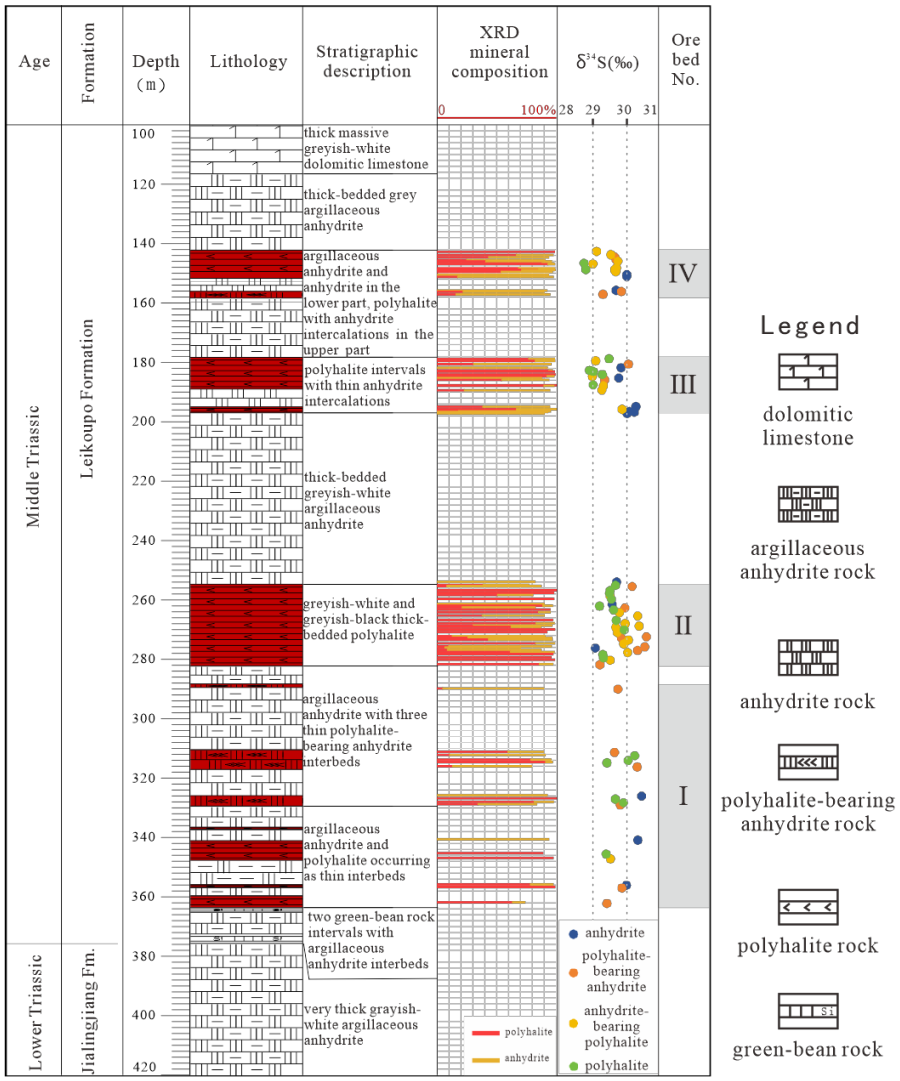


Figure 2. Integrated column of the ore interval in Well LJ1 including lithology, stratigraphic description, XRD, $\delta^{34}S$, and ore bed numbers.

4.1. Macroscopic Characteristics of the Polyhalite Ore

The polyhalite ore occurs in the first member of the Leikoupo Formation (T_2l^1) just above the green-bean rock beds and is closely associated with anhydrite rock. A pronounced alternation rhythm is reflected in the interbedding of polyhalite rock, anhydrite-bearing polyhalite rock, polyhalite-bearing anhydrite rock, and anhydrite rock. Polyhalite

in the study area is dark grey to grey. On the basis of its contact relationships with anhydrite, the polyhalite rock is grouped into four types.

Nodular–banded polyhalite rock consists of nodules and banded lenses of polyhalite or polyhalite–anhydrite aggregates enclosed in a laminated anhydrite matrix that was crumpled by later tectonic compression; metasomatic textures occur along the contacts, and this type forms the main body of the polyhalite ore beds in the study area. Massive polyhalite rock is lithologically homogeneous, structureless and dense, medium- to coarse-crystalline, and is developed only in a few intervals. Laminated polyhalite rock shows a typical sedimentary rhythm of grey polyhalite alternating with greyish-white anhydrite, locally with thin argillaceous and magnesite intercalations; the primary laminae are commonly bent under later compression. Spotted polyhalite rock consists of spotted or star-like polyhalite impregnations and replacements within the anhydrite rock, generally near the contacts between nodular–banded polyhalite rock and anhydrite rock.

4.2. Microfabrics of the Polyhalite Ore Beds

Twenty-seven core thin sections were examined, and four polyhalite microfabric types (PM1–PM4) were distinguished on the basis of their textures, contact relationships and paragenetic positions (Figures 3 and 4).

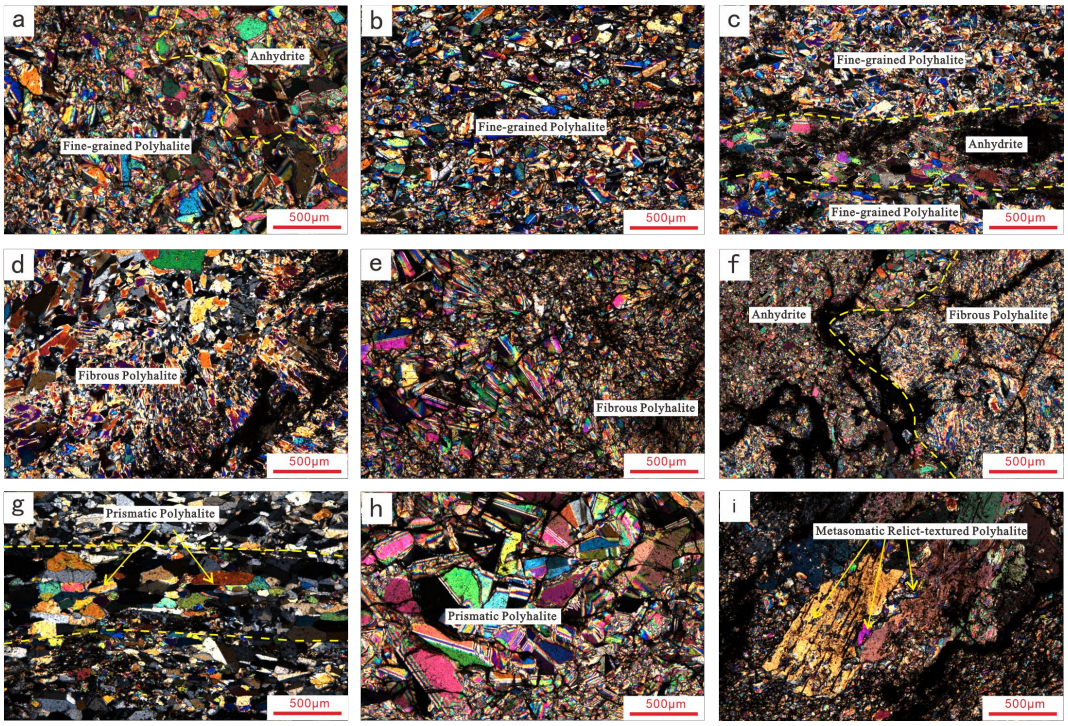


Figure 3. Polyhalite microscopic characteristics discovered in the study area. (**a**) fine-grained polyhalite (PM1) associated with anhydrite; (**b**) uniform fine-grained polyhalite (PM1); (**c**) fine-grained polyhalite (PM1) in laminated polyhalite rock; (**d**,**e**) fibrous polyhalite (PM2); (**f**) fibrous polyhalite (PM2) and the adjacent anhydrite; (**g**) prismatic polyhalite (PM3) associated with granular anhydrite in laminated rock; (**h**) recrystallized prismatic polyhalite (PM3); (**i**) metasomatic relict-textured polyhalite (PM4).

Fine-grained polyhalite (PM1) is a well-sorted granular type (Figures 3a and 4a), 50–200 μm in size, with sharp grain boundaries, polysynthetic twinning and a locally preferred orientation (Figure 3b). It commonly occurs in massive and laminated polyhalite rock (PM1-1), where it may form thin interbeds with anhydrite bounded by sharp, pressure-solved contacts and accompanied by thin argillaceous strips (Figure 3c). It also occurs in the non-boundary parts of nodular–banded rock associated with anhydrite (PM1-2)

(Figure 4c). Fibrous polyhalite (PM2) consists of fine laths arranged in radial aggregates (Figures 3d–f and 4b), a texture regarded as a typical indicator of the replacement of anhydrite by polyhalite [31–33]. Argillaceous material is common in the intercrystalline spaces of the radial aggregates. This type is commonly found at the boundaries of nodular–banded polyhalite rock (Figure 4d), in polyhalite–anhydrite contact zones and in spotted polyhalite rock. Prismatic polyhalite (PM3) comprises coarse crystals with subhedral to euhedral prismatic–platy texture, sharp boundaries, and polysynthetic twinning. This type shows two modes of occurrence: in association with granular anhydrite layers, showing sharp contacts, occasional pressure solution and a marked preferred orientation (PM3-1, Figure 3g), or as late void-filling aggregates in local intercrystalline spaces, with grains coarsening outward from the host (PM3-2, Figure 3h). It occurs only sporadically and does not form the main body of the ore. Metasomatic relict-textured polyhalite (PM4) develops mainly at polyhalite–anhydrite contacts, where polyhalite embays the margins of anhydrite grains or replaces their interiors as patches. Anhydrite even survives only as the original grain outline (Figure 3i). This microfabric type is restricted to spotted polyhalite rock and is a typical product of late-stage metasomatism. For more detailed descriptions of the microscopic characteristics of polyhalite, please refer to Zhang et al. [34].

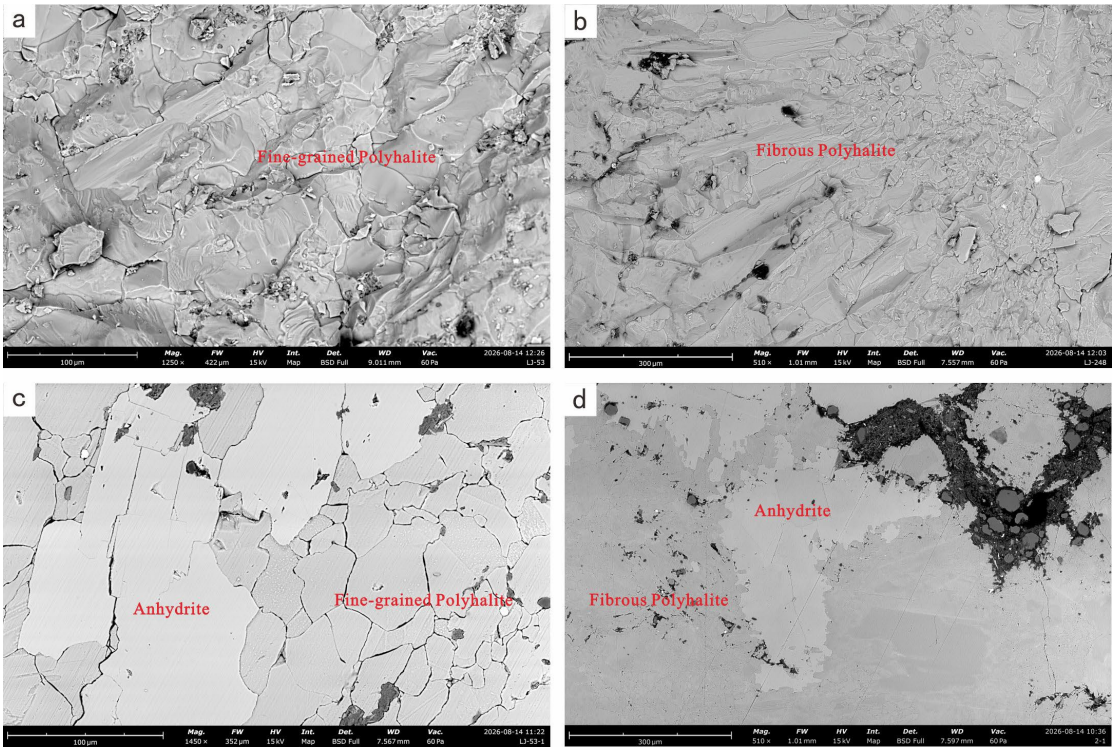


Figure 4. SEM (Scanning electron microscopy) photos of fine-grained polyhalite (**a**,**c**) and fibrous polyhalite (**b**,**d**).

4.3. XRD and SO_4^{2-} Analysis Results

XRD results show that the samples from the ore interval are composed mainly of polyhalite and anhydrite, accompanied by fluctuations in their proportion (Figure 2). A low abundance of magnesite and quartz may be present locally (Figure 5), but they are not shown in Figure 2, as they are not the focus of this study.

The SO_4^{2-} contents of the analyzed samples are listed in Table 1. Because the measurements were made by water dissolution, and polyhalite is considerably more soluble than anhydrite, a higher leached SO_4^{2-} content indicates a higher proportion of polyhalite, and the anhydrite rock shows the lowest SO_4^{2-} content. Combining the qualitative and semi-quantitative constraints from macroscopic and microscopic observations and the

XRD data, the samples fall into four groups (polyhalite rock, anhydrite rock, polyhalite-bearing anhydrite rock, and anhydrite-bearing polyhalite rock). It is worth noting that this nomenclature only covers the two dominant sulfate minerals, polyhalite and anhydrite, which are the key and main components of this study. Minor minerals such as magnesite and quartz are not included in the naming scheme. Accordingly, the terms "polyhalite rock" and "anhydrite rock" indicate that one of the two sulfate minerals dominates that type of rock, while a very small amount of the other sulfate mineral can not be ruled out to be mixed in. Besides, trace amounts of other minerals, e.g., magnesite, quartz, may still occur (Figure 5). The water-soluble SO_4^{2-} content is 31.6%–35.3% for the 23 polyhalite samples and 5.4%–7.6% for the 14 anhydrite samples. For polyhalite-bearing anhydrite samples (n = 20) and anhydrite-bearing polyhalite samples (n = 24), the SO_4^{2-} content ranges from 8.0% to 18.8% and from 21.6% to 30.8%, respectively. XRD patterns of these four types of samples are shown in Figure 5.

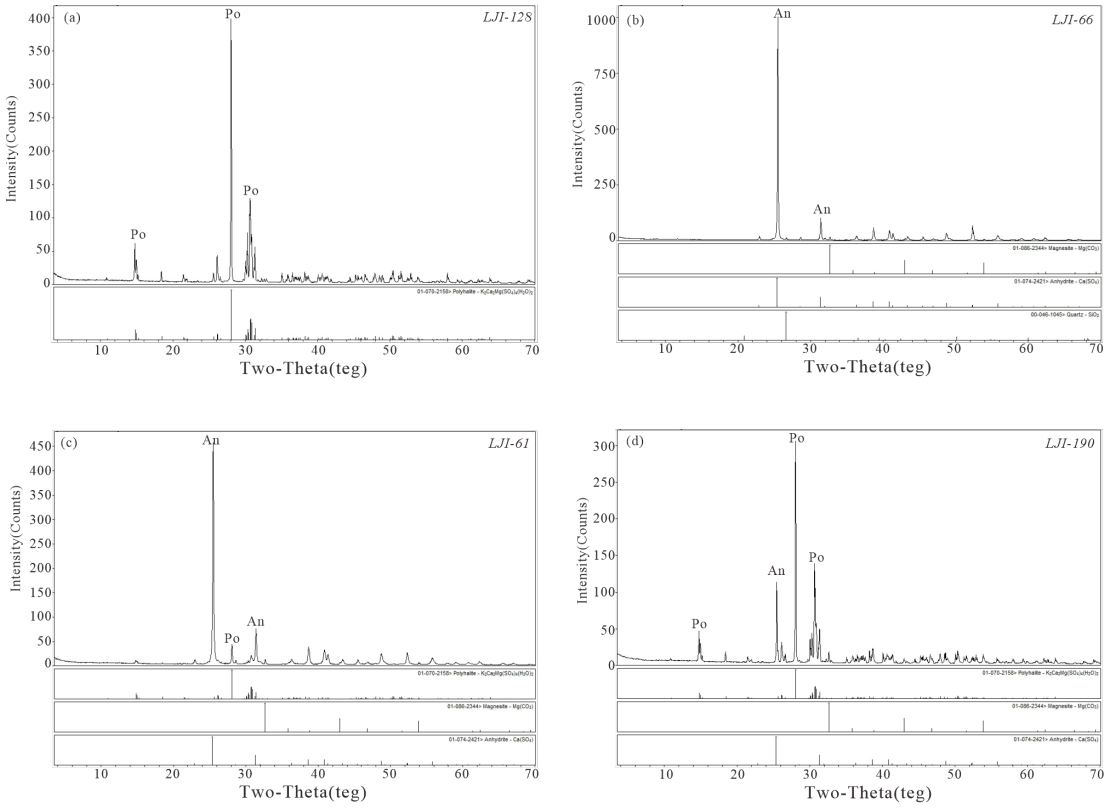


Figure 5. XRD patterns of (**a**) polyhalite sample, (**b**) anhydrite sample, (**c**) polyhalite-bearing anhydrite sample, and (**d**) anhydrite-bearing polyhalite sample.

Table 1. Sulfur isotope and SO_4^{2-} results of samples from Well LJ1.

No.	Samples	Depth (m)	$\delta^{34}S$ (‰)	SO_4^{2-} (%)	Rock Type	Core Bed Number
1	LJ1-2	142.7	29.1	28.5	anhydrite-bearing polyhalite rock	IV
2	LJ1-6	143.8	29.5	23.3	anhydrite-bearing polyhalite rock	IV
3	LJ1-10	144.6	29.6	14.4	polyhalite-bearing anhydrite rock	IV
4	LJ1-15	145.5	29.7	14.1	polyhalite-bearing anhydrite rock	IV

5	LJ1-18	146.0	29.7	21.6	anhydrite-bearing polyhalite rock	IV
6	LJ1-22	146.7	28.7	35.3	polyhalite rock	IV
7	LJ1-23	146.9	29.0	28.1	anhydrite-bearing polyhalite rock	IV
8	LJ1-173	148.3	29.7	26.8	anhydrite-bearing polyhalite rock	IV
9	LJ1-176	148.8	28.8	32.9	polyhalite rock	IV
10	LJ1-177	148.9	29.6	24.3	anhydrite-bearing polyhalite rock	IV
11	LJ1-180	149.5	29.7	23.5	anhydrite-bearing polyhalite rock	IV
12	LJ1-33	150.5	30.0	6.2	anhydrite rock	IV
13	LJ1-36	151.2	30.0	8.4	polyhalite-bearing anhydrite rock	IV
14	LJ1-40	155.8	29.7	7.3	anhydrite rock	IV
15	LJ1-41	156.2	29.8	16.9	polyhalite-bearing anhydrite rock	IV
16	LJ1-46	157.1	29.3	10.8	polyhalite-bearing anhydrite rock	IV
17	LJ1-53	178.8	29.5	32.1	polyhalite rock	III
18	LJ1-56	179.5	29.1	27.9	anhydrite-bearing polyhalite rock	III
19	LJ1-61	180.6	30.0	9.3	polyhalite-bearing anhydrite rock	III
20	LJ1-66	181.8	29.8	5.7	anhydrite rock	III
21	LJ1-70	182.7	28.9	34.5	polyhalite rock	III
22	LJ1-71	183.1	29.0	33.6	polyhalite rock	III
23	LJ1-74	184.1	29.3	33.5	polyhalite rock	III
24	LJ1-77	184.7	29.0	26.5	anhydrite-bearing polyhalite rock	III
25	LJ1-79	185.3	29.7	6.0	anhydrite rock	III
26	LJ1-81	185.9	29.3	17.2	polyhalite-bearing anhydrite rock	III
27	LJ1-90	187.6	29.0	32.4	polyhalite rock	III
28	LJ1-91	187.9	29.3	30.3	anhydrite-bearing polyhalite rock	III
29	LJ1-97	189.4	29.3	25.7	anhydrite-bearing polyhalite rock	III
30	LJ1-101	194.9	30.2	6.3	anhydrite rock	III
31	LJ1-106	195.8	29.8	28.7	anhydrite-bearing polyhalite rock	III
32	LJ1-110	196.5	30.0	5.4	anhydrite rock	III
33	LJ1-111	196.7	30.2	6.3	anhydrite rock	III
34	LJ1-113	197.2	30.0	5.4	anhydrite rock	III
35	LJ1-116	253.9	29.7	5.7	anhydrite rock	II
36	LJ1-121	255.0	29.7	35.0	polyhalite rock	II
37	LJ1-123	255.4	30.1	18.8	polyhalite-bearing anhydrite rock	II
38	LJ1-128	256.8	29.5	35.1	polyhalite rock	II
39	LJ1-133	257.7	29.5	35.1	polyhalite rock	II

40	LJ1-135	258.4	29.5	27.0	anhydrite-bearing polyhalite rock	II
41	LJ1-141	259.7	29.5	34.4	polyhalite rock	II
42	LJ1-147	261.4	29.6	5.9	anhydrite rock	II
43	LJ1-150	262.0	29.2	33.2	polyhalite rock	II
44	LJ1-154	262.6	29.9	16.4	polyhalite-bearing anhydrite rock	II
45	LJ1-158	263.3	29.6	31.6	polyhalite rock	II
46	LJ1-162	264.2	29.8	28.7	anhydrite-bearing polyhalite rock	II
47	LJ1-167	265.3	30.3	29.6	anhydrite-bearing polyhalite rock	II
48	LJ1-185	266.8	29.7	32.8	polyhalite rock	II
49	LJ1-190	267.9	29.9	28.2	anhydrite-bearing polyhalite rock	II
50	LJ1-194	268.7	30.3	25.7	anhydrite-bearing polyhalite rock	II
51	LJ1-196	269.1	29.7	30.8	anhydrite-bearing polyhalite rock	II
52	LJ1-199	270.0	29.9	34.2	polyhalite rock	II
53	LJ1-204	270.9	29.7	28.8	anhydrite-bearing polyhalite rock	II
54	LJ1-209	272.3	30.5	12.8	polyhalite-bearing anhydrite rock	II
55	LJ1-212	272.8	29.8	9.4	polyhalite-bearing anhydrite rock	II
56	LJ1-215	273.4	30.0	22.1	anhydrite-bearing polyhalite rock	II
57	LJ1-220	274.7	29.9	26.3	anhydrite-bearing polyhalite rock	II
58	LJ1-225	275.7	30.5	17.8	polyhalite-bearing anhydrite rock	II
59	LJ1-227	276.1	29.1	6.7	anhydrite rock	II
60	LJ1-231	276.9	30.3	8.6	polyhalite-bearing anhydrite rock	II
61	LJ1-234	277.6	30.0	28.1	anhydrite-bearing polyhalite rock	II
62	LJ1-238	278.3	29.3	34.7	polyhalite rock	II
63	LJ1-243	279.4	29.3	32.9	polyhalite rock	II
64	LJ1-248	280.2	29.5	29.7	anhydrite-bearing polyhalite rock	II
65	LJ1-256	281.7	29.2	9.9	polyhalite-bearing anhydrite rock	II
66	LJ1-265	289.9	29.7	13.8	polyhalite-bearing anhydrite rock	II
67	LJ1-272	311.2	29.6	8.4	polyhalite-bearing anhydrite rock	I
68	LJ1-277	312.3	30.2	34.0	polyhalite rock	I
69	LJ1-285	313.9	30.0	33.9	polyhalite rock	I
70	LJ1-289	314.7	29.4	33.3	polyhalite rock	I
71	LJ1-296	316.1	30.3	14.9	polyhalite-bearing anhydrite rock	I

72	LJ1-298	325.9	30.4	6.8	anhydrite rock	I
73	LJ1-302	326.9	29.7	34.2	polyhalite rock	I
74	LJ1-307	328.1	29.9	33.1	polyhalite rock	I
75	LJ1-311	328.9	29.8	13.0	polyhalite-bearing anhydrite rock	I
76	LJ1-321	340.7	30.3	6.3	anhydrite rock	I
77	LJ1-329	345.4	29.4	32.4	polyhalite rock	I
78	LJ1-336	347.0	29.5	29.7	anhydrite-bearing polyhalite rock	I
79	LJ1-341	355.9	30.0	7.6	anhydrite rock	I
80	LJ1-347	356.8	29.8	18.2	polyhalite-bearing anhydrite rock	I
81	LJ1-353	362.0	29.4	8.0	polyhalite-bearing anhydrite rock	I

4.4. Sulfur Isotope Results

Sulfur isotopes were measured on the sulfate samples from well LJ1 and the results are listed in Table 1. The average $\delta^{34}S$ value of all samples is 29.67 ± 0.41 ‰, ranging from 28.7 ‰ to 30.5 ‰ (Table 1). Based on the above-mentioned classification of samples from core observation, thin-section examination, XRD and water-soluble SO_4^{2-} content, the polyhalite samples have $\delta^{34}S$ values of 28.7–30.2 ‰, with an average of 29.43 ± 0.38 ‰; the anhydrite samples have $\delta^{34}S$ values of 29.1–30.4 ‰, with an average of 29.91 ± 0.33 ‰; the polyhalite-bearing anhydrite samples have $\delta^{34}S$ values of 29.2–30.5 ‰, with an average of 29.83 ± 0.37 ‰; and the anhydrite-bearing polyhalite samples have $\delta^{34}S$ values of 29.0–30.3 ‰, with an average of 29.62 ± 0.36 ‰. The $\delta^{34}S$ values differ slightly between ore beds. Samples from ore beds I and II both average 29.8 ‰, while those from ore beds III and IV both average 29.5 ‰ (Figure 6a).

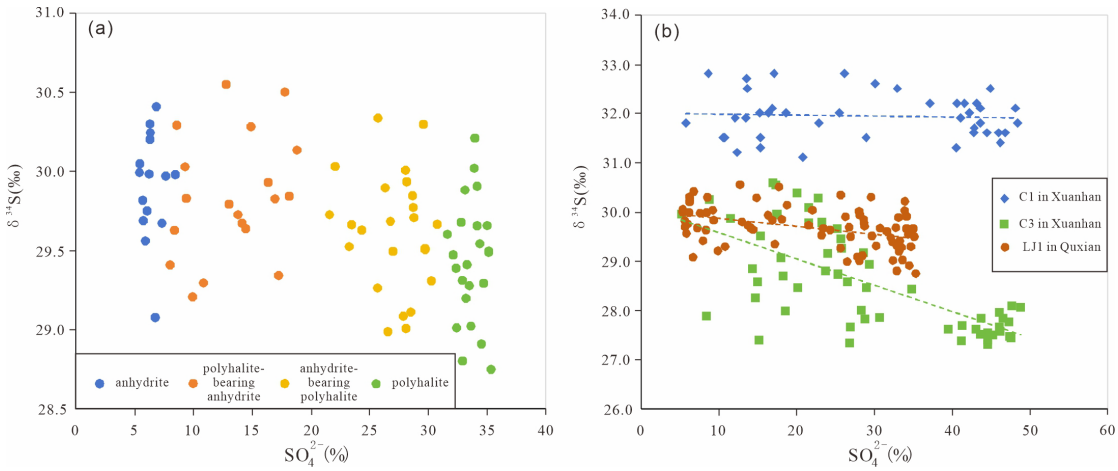


Figure 6. Scatter plot of $\delta^{34}S$ & SO_4^{2-} of (**a**) selected sulfate samples of different kinds from well LJ1 and (**b**) sulfate samples from different wells.

In addition to the evaporites of the study area, data from the adjacent Xuanhan area, where polyhalite is associated with halite, were used for comparison. The sulfur isotope and SO_4^{2-} data come from two polyhalite-bearing wells in the Xuanhan area, wells C1 and C3, which provide 41 and 56 data sets, respectively. These data are reported by Zuo et al. [35].

5. Discussion

5.1. Sedimentological Evidence for the Genesis of Polyhalite

The genesis of the polyhalite associated with anhydrite in the Quxian area has long been debated. Previous research, on the basis of the sedimentary characteristics of the polyhalite, has mostly supported a metasomatic origin [11,18,36,37], whereas a few have argued that the polyhalite in this area may have formed by primary deposition [38]. Combining the macroscopic and microscopic evidence, and building on the polyhalite microfabrics classification, it is considered that the different polyhalite types in the study area clearly formed in more than one stage.

Fine-grained polyhalite (PM1) has sharp boundaries and shows no metasomatic relict textures or any evidence of an earlier precursor mineral. It commonly preserves the primary laminae intact, and is therefore interpreted as primary or penecontemporaneous in origin [39–41]. Because the polyhalite in the study area is mainly associated with anhydrite, and the brine never reached the halite precipitation stage, the depositional environment is best assigned to the tidal-flat facies of an evaporite platform (Figure 7a). Ca^{2+} and SO_4^{2-} were abundant in this system, so an effective supply of K^+ and Mg^{2+} would have been enough to satisfy the hydrochemical conditions for polyhalite precipitation [41]. The brine in the study area never became concentrated enough for halite precipitation, but large volumes of rock salt and of primary polyhalite associated with halite are developed in the salt salterns of the adjacent Nanchong and Xuanhan areas. It has been shown that repeated evaporation and concentration had already raised the K^+ and Mg^{2+} concentrations of the brine in those areas to relatively high levels, so that these areas can be regarded as the source of K^+ and Mg^{2+} for the study area [19,35,42]. The brine may have been driven into the study area by tectonic uplift, or simply by subsurface seepage. When the K^+- and Mg^{2+}-rich brine supplied from the adjacent areas mixed with the Ca^{2+} and SO_4^{2-} released by evaporation of the local brine or by dissolution of previously precipitated gypsum or anhydrite, the hydrochemical conditions for polyhalite precipitation were achieved (Figure 7b). Based on the dirty appearance and rosettes of anhydrite under the microscope, the Early-Middle anhydrite in the Sichuan Basin was suggested to have formed most likely by the dehydration of gypsum [32,35]. However, this process is not the focus of the present study. Therefore, for the sake of rigor, throughout this paper we refer to the early sulfate precipitates as gypsum/anhydrite. This produced the laminated and massive polyhalite rocks that consist mainly of fine-grained polyhalite. This interpretation is consistent with the results of laboratory simulations of the chemical conditions. Phase-equilibrium experiments and thermodynamic simulations show that primary polyhalite cannot form by direct evaporation and concentration of seawater unless suitable external recharge is supplied during evaporation [43–47]. The fine-grained polyhalite in the nodular–banded polyhalite rock may record incomplete dissolution of primary gypsum or anhydrite layers, which left local relics of the sulfate rock. Penecontemporaneous polyhalite was then deposited in the same layer as banded lenses together with these relics.

Fibrous polyhalite (PM2) and metasomatic relict-textured polyhalite (PM4) usually develop at the contacts between polyhalite rock and anhydrite rock. The felty and radial habits of the fibrous polyhalite are regarded as preserving the original morphology of the anhydrite, and are commonly taken as typical evidence of a metasomatic origin [31–33,48]. In the metasomatic relict-textured polyhalite, the newly formed polyhalite clearly coexists with the anhydrite that it replaced, and the distinct grain-boundary erosion and intragranular patchy dissolution features attest to their link with later fluid infiltration [33,49]. These two types are therefore interpreted as products of the replacement of anhydrite by post-diagenetic K^+- and Mg^{2+}-rich fluids, and they formed later than the fine-grained polyhalite (Figure 7d) [50].

The minor prismatic polyhalite associated with granular anhydrite layers (PM3-1) shows no impregnation of the surrounding anhydrite. Its euhedral habit and marked bedding-parallel arrangement indicate that it formed when K^+- and Mg^{2+}-rich brine from an adjacent horizon (possibly released by partial dissolution of a neighboring polyhalite layer) mixed with the anhydrite sediment during the penecontemporaneous stage (Figure 7c). The common association with fine-grained polyhalite in laminated polyhalite rock supports this interpretation. Where prismatic polyhalite occurs between, or locally within, fine-grained polyhalite layers and between fibrous aggregates (PM3-2), the grains become progressively coarser, which points to later growth and indicates recrystallization within locally dissolved spaces.

In summary, both primary and penecontemporaneous processes and later metasomatism by diagenetic fluids contributed to the formation of the shallow polyhalite potash deposit in the study area.

5.2. Implications of Sulfur Isotopes for the Genesis of Polyhalite

The $\delta^{34}S$ values of brine in evaporites can be influenced by three factors: bacterial sulfate reduction (BSR), the source of SO_4^{2-}, and the precipitation of sulfate minerals that incorporate ^{34}S [51–53]. Studies of evaporite basins worldwide have revealed anomalously high $\delta^{34}S$ values (generally 27–28 ‰, up to 32 ‰) in the Early Triassic and the early Middle Triassic, following a sudden jump at the beginning of the period ($\delta^{34}S$: 10 – 13 ‰) [54–61]. After the end-Permian mass extinction, the global environment was in an anoxic state accompanied by abnormal marine conditions [59,62,63]. During this period, deep seawater was widely characterized by hydrogen sulfide (H_2S) enrichment, which formed a pronounced stratification with the surface water [64,65]. Anaerobic bacteria proliferated extensively under these global anoxic conditions. Preferential consumption of ^{32}S by BSR resulted in enrichment of ^{34}S in the deep water [51–53,58]. Because BSR mainly operates in the anoxic deep-water environment, the prominent $\delta^{34}S$ anomaly with such a large difference ($\delta^{34}S$: more than 15 ‰) in shallow-water evaporites replenished by periodic seawater supply cannot be mainly attributed to strong local BSR effects. This is also inconsistent with the global nature of the phenomenon. The abrupt change in $\delta^{34}S$ of the shallow-marine evaporites is therefore attributed to a sudden upwelling of ^{34}S-rich deep water [59,66]. Newton et al. [57] proposed that the sulfur isotope anomaly in the Early Triassic and early Middle Triassic can be regarded as a geochemical "fossil" of the anoxic event. BSR linked to global perturbations in the marine environment set the baseline for globally high $\delta^{34}S$ values.

The $\delta^{34}S$ values of the evaporites in the study area agree with the high values recorded in other regions at that time, which indicates that the SO_4^{2-} was derived from globally ^{34}S-enriched seawater. This also suggests that the polyhalite in the study area either formed by primary or penecontemporaneous deposition, or formed by metasomatism in which seawater of the same source acted as the diagenetic fluid. Meteoric water generally has $\delta^{34}S$ values of about 10 ‰, and sulfates influenced by volcanic activity range from −10 ‰ to 10 ‰. The $\delta^{34}S$ values would show a clear decrease if such external sources supplied the diagenetic fluids [17].

In the study area, the $\delta^{34}S$ values of polyhalite (29.43 ± 0.38 ‰, $n = 23$) are lower than those of anhydrite (average 29.91 ± 0.33 ‰, $n = 14$) (Welch t-test, $p < 0.001$; difference: 0.48 ‰). Given that the grouping was based on macroscopic and microscopic examination and XRD, admixture of a small amount of the other mineral would only make the difference between pure polyhalite and anhydrite smaller than its true value. Therefore, the difference of 0.48 ‰ between the two groups should be taken as a minimum estimate; the sulfur isotopic fractionation between pure polyhalite and anhydrite would be greater than this difference. The $\delta^{34}S$ values of anhydrite-bearing polyhalite rock and polyhalite-bearing

anhydrite rock lie between the two end members, which further supports this point. Statistical results also confirm, with over 99.9% confidence ($p < 0.001$), that a systematic difference in $\delta^{34}S$ indeed exists between polyhalite and anhydrite, rather than being a chance result caused by sampling or analytical error. The $\delta^{34}S$ difference between polyhalite and anhydrite relates to the third factor mentioned above, which is that the precipitation of sulfate minerals modifies the sulfur isotope composition of the brine. Sulfate precipitation preferentially consumes ^{34}S from the brine, so sulfur isotope values decrease from the sulfate stage to the halite stage [67,68]. Anhydrite precipitated directly from evaporated brine in the tidal-flat setting, whereas polyhalite required recharge from more strongly evaporated, K^+- and Mg^{2+}-rich brine from the adjacent area. Because the recharge brine had already lost ^{34}S during earlier sulfate precipitation, its $\delta^{34}S$ should be lower, which accounts for the lower $\delta^{34}S$ of the polyhalite. Polyhalite in the Xuanhan area also shows the same negative correlation (Figure 6b).

The difference between the two minerals, however, varies from area to area, which reflects different degrees of fluctuation in the depositional environment. In well C3 of the Xuanhan area the difference in $\delta^{34}S$ between anhydrite and polyhalite is the largest, because the depositional record there covers a wide range from the dolomite flat of a restricted platform to the salt lake of an evaporite platform. The difference is smallest in well C1 of the Xuanhan area, where the overall degree of evaporation was higher and the samples were mainly collected from the salt lake of the evaporite platform and the adjacent gypsum/anhydrite lake [35]. The Quxian area lies between these two extremes, which further supports the interpretation that the polyhalite associated with anhydrite in the study area formed in an individual tidal-flat setting on the evaporite platform that was recharged from the surrounding salt lakes on the evaporite platform.

In addition, although the sulfur isotope values of the evaporites in the different areas all accord with the globally high values, their absolute ranges differ to some extent. The $\delta^{34}S$ values of well C1 are higher than those of well C3, and the values for the Quxian area lie between them (Figure 6b). Judging from the depositional setting, the polyhalite in the Xuanhan area is associated with halite and developed in gypsum–salt lakes with a higher degree of evaporation; earlier sulfate precipitation consumed more ^{34}S, so its $\delta^{34}S$ should be lower than that in the Quxian area. Well C3 matches this expectation, but the $\delta^{34}S$ values of well C1 are higher than those of both well C3 and the evaporites of the Quxian area. Sedimentological research shows that the depositional area of well C1 has the highest content and the greatest thickness of rock salt, which means this location experienced the strongest overall evaporation and was closer to the terrestrial source direction [35]. Therefore, if it had been influenced by the source of SO_4^{2-}, $\delta^{34}S$ values would only have been lower rather than higher, similar to the effect of sulfate precipitation mentioned above [51–53]. Therefore, this may also only be related to the degree of closure of the local depositional environment. Local bacterial reduction in shallow water may have consumed more ^{32}S from the brine, raising its $\delta^{34}S$ (~2–3‰) above that of other parts of the Sichuan Basin.

The $\delta^{34}S$ characteristics also differ among different ore beds. In ore beds I, III and IV, the $\delta^{34}S$ values of polyhalite and anhydrite samples differ by 0.47 ± 0.18 ‰ (mean ± 1 s.e.) in bed I, 0.84 ± 0.14 ‰ in bed III and 1.10 ± 0.16 ‰ in bed IV, whereas no resolvable difference is found in bed II (−0.05 ± 0.20 ‰), where the anhydrite control is weakest ($n = 3$) (Figure 2). Because whole-rock $\delta^{34}S$ is a modal-weighted average that covaries with SO_4^{2-} content and rock type, these patterns are accordingly reported as an observation compatible with the textural interpretation.

In summary, sulfur isotope analysis of the evaporites provides important evidence on the sources of the ore-forming material and on the genetic model of the polyhalite. This study further demonstrated, through a combination of methods, the genesis of polyhalite in the Quxian area that had puzzled researchers for years, providing important evidence

for the exploration and development of marine potash in China. Furthermore, it also provides a reference for the study and interpretation of similar potash deposits worldwide.

Geochemical studies of individual minerals at the microscopic scale remain a limitation of the current research and will be the direction of follow-up work.

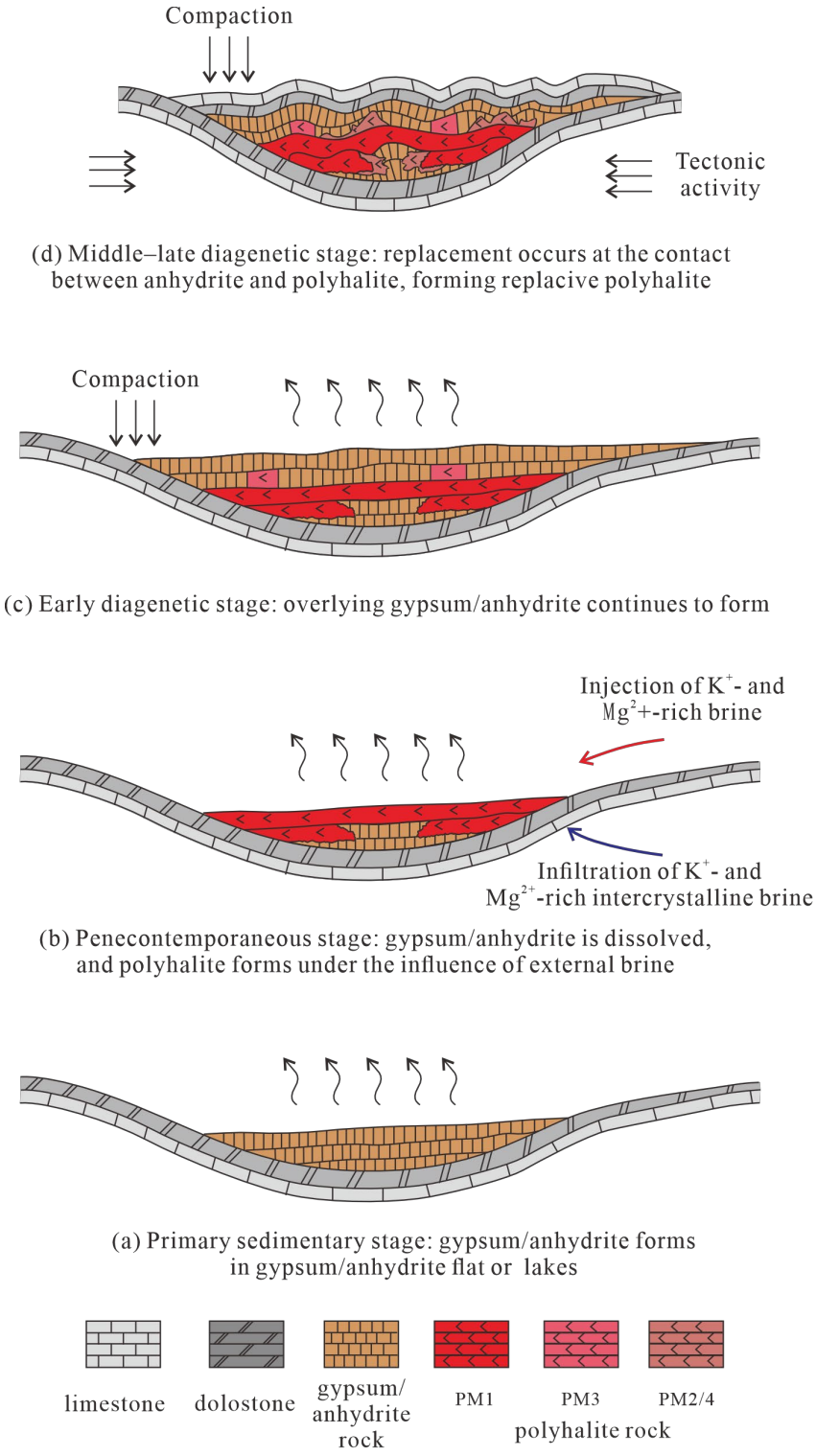


Figure 7. Genetic model of Triassic polyhalite in the Quxian area, northeastern Sichuan Basin.

https://doi.org/10.3390/min16121229

6. Conclusions

(1) The polyhalite-bearing potash ore intervals in the Quxian area comprise four macroscopic rock types consisting mainly of polyhalite and anhydrite, in which the polyhalite mineral exhibits four microfabrics (PM1–PM4).

(2) A genetic model involving several formation stages has been established for the polyhalite: fine-grained polyhalite (PM1) and part of the prismatic polyhalite (PM3-1) are of primary or penecontemporaneous origin through the input of K^+- and Mg^{2+}-rich brine, whereas fibrous (PM2) and metasomatic relict-textured (PM4) polyhalite, as well as other prismatic polyhalite (PM3-2) record later replacement or recrystallization, so that both primary/penecontemporaneous precipitation and later metasomatism contributed to the formation of the potash deposit.

(3) The $\delta^{34}S$ values (28.7–30.5 ‰, average 29.7 ‰) of evaporite in the study area agree with the globally high Early Triassic values and indicate a ^{34}S-enriched seawater source. The comparison of $\delta^{34}S$ among different minerals and among evaporites from different regions in Sichuan Basin provides new evidence for the genesis of the shallow polyhalite in the Quxian area of the Sichuan Basin.

Author Contributions: Conceptualization, Y.Z. and F.Z.; methodology, F.Z.; software, B.G. and F.Z.; validation, E.X. and X.N.; investigation, B.G. and Y.Z.; resources, B.G. and Y.Z.; data curation, F.Z.; writing—original draft preparation, F.Z.; writing—review and editing, Y.Z., F.Z. and E.X.; visualization, B.G.; supervision, Y.Z.; project administration, K.S. and Y.Z.; funding acquisition, K.S. All authors have read and agreed to the published version of the manuscript.

Funding: This study was supported by the National Key Research and Development Program of China "Metallogenic law, exploration technology and demonstration of storage increase of new type of polyhalite potassium salt deposits in Northeast Sichuan" (Grant number: 2023YFC2906503) and the China Geological Survey Program "Investigation and Evaluation of Marine Potash and Lithium Salt Resources in the Northeastern Sichuan Basin and Tarim Basin" (Grant number: DD202602109305).

Data Availability Statement: The data supporting the findings of this study are presented in the article.

Acknowledgments: We thank Xiang Li and Xiaomiao Li for their help in sample collection.

Conflicts of Interest: The authors declare no conflicts of interest.

References

1. Horita, J.; Friedman, T.J.; Lazar, B.; Holland, H.D. The composition of Permian seawater. *Geochim. Cosmochim. Acta* **1991**, *55*, 417–432.
2. Garland, J.; Tiltman, C.; Inglis, C. Sedimentology, palaepgeography and diagenesis of the Upper Permian (Z2) Hauptdolomit Formation on the southern margin of the Mid Norrth Sea High and implications for reservior prospectivity. *J. Pet. Geol.* **2023**, *46*, 329–360.
3. Peryt, T.M.; Tomassi-Morawiec, H.; Czapowski, G.; Hryniv, S.P.; Pueyo, J.J.; Eastoe, C.J.; Vovnyuk, V. Polyhalite occurrence in the Werra (Zechstein, Upper Permian) Peribaltic Basin of Poland and Russia: Evaporite facies constraints. *Carbonates Evaporites* **2005**, *20*, 182–194.
4. Zheng, M.; Yuan, H.; Zhang, Y.; Liu, X.; Chen, W.; Li, J. Regional distribution and prospects of potash in China. *Acta Geol. Sin.* **2010**, *84*, 1523–1553. (In Chinese with English abstract)
5. Jin, F. Enlightenment to China from the exploitation and utilization of halite resources abroad. *Chem. Min. Technol.* **1989**, *3*, 31–34. (In Chinese with English abstract)
6. Cai, K.; Yuan, J. Metallogenic conditions and prospecting direction of Triassic potash in Sichuan. *Geol. Chem. Miner.* **1986**, *2*, 1–9. (In Chinese)

7. Lin, Y.; Chen, S. Discussion on the evaporite generating modes, salt-forming mechanism and potassium-hunting prospect of the Lower–Middle Triassic in the Sichuan Basin. *J. Salt Lake Res.* **2008**, *16*, 1–10. (In Chinese with English abstract)
8. Zheng, M.; Zhang, Y.; Shang, W.; Xing, E.; Zhong, J.; Gui, B.; Peng, Y. Discovery of a new type of polyhalite potassium ore in the Puguang region, northeastern Sichuan. *Geol. China* **2018**, *45*, 1074–1075. (In Chinese with English abstract)
9. Liao, L.; Huang, F.; Liu, Q.; Hu, C. The characteristics and origins of polyhalite in gypsum-anhydrite deposits in Nongle area, eastern Sichuan. *Miner. Rocks* **1984**, 4, 94–100. (In Chinese with English abstract)
10. Li, Y.; Han, T. An experimental study on the formative conditions of polyhalite in the Triassic of the Sichuan Basin. *Geoscience* **1987**, *1*, 400–411. (In Chinese with English abstract)
11. Lin, C. Metamorphic evolution of K-bearing rock series of the Triassic and implication in search for potash salt in Sichuan Basin. *Acta Geol. Sichuan* **1994**, *14*, 122–129. (In Chinese with English abstract)
12. Li, Y.; Cai, K.; Han, T. Origin of potassium-rich brine and the metamorphism of Triassic evaporites in the Sichuan Basin. *Geoscience* **1998**, *12*, 222–227. (In Chinese with English abstract)
13. Zhong, J.; Zheng, M.; Tang, X.; Liu, Z.; Wang, F.; Cai, C.; Pang, B. Sedimentary characteristics of deep polyhalite in the Huangjinkou anticline of northeastern Sichuan and its genetic study. *Miner. Depos.* **2018**, *37*, 81–90. (In Chinese with English abstract)
14. Zhong, J.; Zheng, M.; Zhang, Y.; Tang, X.; Zhang, X. Sedimentary and geochemical characteristics of Triassic new type of polyhalite potassium resources in northeastern Sichuan and its genetic study. *Sci. Rep.* **2020**, *10*, 13528.
15. Zhao, Y.; Liu, C.; Ding, T.; Gonzalez, L.A.; Li, Z.; Wang, M.; Wang, L.; Zhu, Z. Origin and depositional paleoenvironment of Triassic polyhalite in the Jialingjiang Formation, Sichuan Basin. *Carbonates Evaporites* **2020**, *35*, 64.
16. Zhang, X.; Zhu, Z.; Cui, Z.; Zhao, Y.; He, C.; Hu, F.; Wang, K. Genesis of polyhalite and its significance of the Jialingjiang Formation in the Dianjiang Salt Basin, eastern Sichuan Basin. *Earth Sci.* **2022**, *47*, 27–35.
17. Gong, D.; Xiao, B.; Bagas, L.; Die, L.; Zhou, J.; Zou, H. Origin of the Early to Middle Triassic polyhalite minerals in the Sichuan Basin, SW China: New evidence from calcium and sulfur isotopes and microfabrics. *Ore Geol. Rev.* **2021**, *139*, 104439.
18. Hou, X.; Gong, D.; Wen, H.; Li, C.; Hui, B.; Zhang, H.; Zhou, J.; Li, J. Study on the temporal and spatial distribution, microscopic characteristics and genesis of Triassic polyhalite in the Sichuan Basin. *Geol. Rev.* **2020**, *66*, 1555–1571. (In Chinese with English abstract)
19. Zhang, Y.; Xing, E.; Zheng, M.; Su, K.; Gui, B.; Zhong, J.; Zuo, F.; Shang, W.; Niu, X.; Wang, N.; et al. Discovery, breakthrough and prospect of the "new type polyhalite potash deposit" in the Puguang area, northeastern Sichuan Basin. *Acta Geol. Sin.* **2024**, *98*, 2823–2846. (In Chinese with English abstract)
20. Scotese, C.R. *Atlas of Permo-Triassic Paleogeographic Maps (Mollweide Projection), Maps 43-52, Vols. 3 & 4 of the PALEOMAP Atlas for ArcGIS;* PALEOMAP Project: Evanston, IL, USA, 2014; maps 48. doi.org/10.13140/2.1.2609.9209
21. Huang, H.; He, D.; Li, Y.; Fan, H. Determination and formation mechanism of the Luzhou paleo-uplift in the southeastern Sichuan Basin. *Earth Sci. Front.* **2019**, *26*, 102–120. (In Chinese with English abstract)
22. He, D.; Li, D.; Zhang, G.; Zhao, L.; Fan, C.; Lu, R.; Wen, Z. Formation and evolution of multi-cycle superposed Sichuan Basin, China. *Chin. J. Geol.* **2011**, *46*, 589–606. (In Chinese with English abstract)
23. Zhao, Y.; Liu, C.; Gong, D.; Zhou, J.; Ding, T.; Wang, M.; Wang, L. The Luzhou–Kaijiang paleo-uplift control on the formation environments of Triassic salt and potassium deposits in eastern Sichuan. *Acta Geol. Sin.* **2015**, *89*, 1983–1989. (In Chinese with English abstract)
24. Warren, J.K. Evaporites through time: Tectonic, climatic and eustatic controls in marine and nonmarine deposits. *Earth-Sci. Rev.* **2010**, *98*, 217–268.
25. Williams, M.; Haywood, A.M.; Gregory, F.J.; Schmidt, D.N. *Deep-Time Perspectives on Climate Change: Marrying the Signal from Computer Models and Biological Proxies*; The Geological Society: London, UK, 2007; 595p.
26. Qian, L.; Shi, Z.; Ou, L. Research advances in Permian–Triassic paleoclimate: Formation, development and decline of Pangaean Megamonsoon. *Mar. Orig. Pet. Geol.* **2010**, *15*, 52–58. (In Chinese with English abstract)
27. Sun, Y.; Joachimski, M.M.; Wignall, P.B.; Yan, C.; Chen, Y.; Jiang, H.; Wang, L.; Lai, X. Lethally hot temperatures during the Early Triassic greenhouse. *Science* **2012**, *338*, 366–370.
28. Lin, Y.; Bian, M. Distribution of carbonate component as salt-forming mark in Triassic evaporite in the Sichuan Basin. *Geol. Chem. Miner.* **2001**, *23*, 57–61. (In Chinese with English abstract)
29. Lin, Y.; Zheng, M.; Zhang, Y.; Xing, E.; Redfern, S.A.T.; Xu, J.; Zhong, J.; Niu, X. Mineralogical and geochemical characteristics of Triassic lithium-rich K-bentonite deposits in Xiejiacao Section, South China. *Minerals* **2020**, *10*, 69.
30. Zhu, Z.; Wang, G. Paleogeography of before and after deposition of green-bean rock (altered tuff) between the Early and Middle Triassic in the Upper Yangtze Platform and its adjacent areas. *Oil Gas Geol.* **1986**, *7*, 344–355. (In Chinese with English abstract)

31. Peryt, T.M.; Pierre, C.; Gryniv, S.P. Origin of polyhalite deposits in the Zechstein (Upper Permian) Zdrada platform (northern Poland). *Sedimentology* **1998**, *45*, 565–578.
32. Leitner, C.; Wiesmaier, S.; Köster, M.H.; Gilg, H.A.; Finger, F.; Neubauer, F. Alpine halite–mudstone–polyhalite tectonite: Sedimentology and early diagenesis of evaporites in an ancient rift setting (Haselgebirge Formation, eastern Alps). *GSA Bull.* **2017**, *129*, 1537–1553.
33. Schorn, A.; Neubauer, F.; Genser, J.; Bernroider, M. Polyhalite microfabrics in an Alpine evaporite mélange: Hallstatt, eastern Alps. *J. Struct. Geol.* **2013**, *46*, 57–75.
34. Zhang, Y.; Zheng, M.; Gui, B.; Zuo, F.; Lin, Y.; Xing, E.; Su, K.; Luo, Y.; Peng, Y.; Nie, Z.; et al. A new breakthrough in prospecting for shallow polyhalite potassium ore in the marine strata of Well Lejia-1 in Quxian area, northeastern Sichuan Basin. *Miner. Depos.* **2026**, *45*, 1–9. (In Chinese with English abstract)
35. Zuo, F.; Zhang, Y.; Gui, B.; Su, K.; Xing, E.; Niu, X.; Peng, Y.; Xue, Y. Sedimentary evolution under high-frequency sea-level oscillations of the Lower Triassic carbonate–evaporite system in the Xuanhan area, Sichuan Basin: Implications for the genesis of polyhalite minerals. *Sediment. Geol.* **2026**, *494*, 107032.
36. Pan, Z. A preliminary study on the genesis of polyhalite in the Lower–Middle Triassic of Nongle, Quxian, Sichuan. *Geol. Build. Mater.* **1988**, *1*, 6–11. (In Chinese)
37. Lin, Y.; Yin, S. Distribution, genesis and significance of the shallow-seated polyhalite ore in Quxian, Sichuan. *Acta Geol. Sichuan* **1998**, *18*, 121–125. (In Chinese with English abstract)
38. Huang, X. The first polyhalite deposit in China. *Yunnan Geol.* **1996**, *15*, 52–61. (In Chinese)
39. Steward, F.H. The Permian lower evaporites of Fordon in Yorkshire. *Proc. Yorks. Geol. Soc.* **1963**, *34*, 1–44.
40. Colter, V.S.; Reed, G.E. Zechstein 2 Fordon evaporites of the Atwick No. 1 borehole, surrounding areas of N.E. England and the adjacent southern North Sea. *Contrib. Sedimentol.* **1980**, *9*, 115–129.
41. Biehl, B.C.; Reuning, L.; Strozyk, F.; Kukla, P.A. Origin and deformation of intra-salt sulphate layers: An example from the Dutch Zechstein (Late Permian). *Int. J. Earth Sci.* **2014**, *103*, 697–712.
42. Bai, C.; Liu, J. Formation conditions of Lower–Middle Triassic polyhalite in Nanchong Salt Basin, Sichuan and its potassium prospecting significance. *Ground Water* **2022**, *44*, 174–177. (In Chinese with English abstract)
43. Braitsch, O. *Salt Deposits: Their Origin and Composition*; Springer: Berlin, Germany, 1971; 297p.
44. Han, W.; Gu, S.; Cai, K. On the formative conditions of polyhalite in the six-component system K^+, Na^+, Mg^{2+}, Ca^{2+}//Cl^-, SO_4^{2-}–H_2O. *Chin. Sci. Bull.* **1982**, *27*, 362–365. (In Chinese)
45. Freyer, D.; Voigt, W. Crystallization and phase stability of $CaSO_4$ and $CaSO_4$-based salts. *Monatsh. Chem.* **2003**, *134*, 693–719.
46. Wollmann, G. Crystallization Fields of Polyhalite and Its Heavy Metal Analogues. Ph.D. Thesis, University Bergakademie Freiberg, Freiberg, Germany, 2010.
47. Li, D.; Gao, D.; Bian, S.; Li, W.; Dong, Y. Revisiting the crystallization field of polyhalite in the Na^+, K^+, Mg^{2+}, Ca^{2+}//Cl^-, SO_4^{2-}–H_2O system. *Earth Sci. Front.* **2021**, *28*, 46–55. (In Chinese with English abstract)
48. Balzer, D. Mikrofazies-Analyse von Ca-Sulfatgesteinen des Zechstein. *Geol. Jahrb. Reihe D* **1997**, *106*, 99.
49. Boschetti, T.; Cortecci, G.; Toscani, L.; Iacumin, P. Sulfur and oxygen isotope compositions of Upper Triassic sulfates from Northern Apennines (Italy): Palaeogeographic and hydrogeochemical implications. *Geol. Acta* **2011**, *9*, 129–147.
50. Harlov, D.E.; Austrheim, H. Metasomatism and the chemical transformation of rock: Rock–mineral–fluid interaction in terrestrial and extraterrestrial environments. In *Lecture Notes in Earth System Sciences*; Springer: Berlin, Germany, 2012; pp. 1–16.
51. Holser, W.T.; Kaplan, I.R. Isotope geochemistry of sedimentary sulfates. *Chem. Geol.* **1966**, *1*, 93–135.
52. Habicht, K.S.; Canfield, D.E.; Rethmeier, J. Sulfur isotope fractionation during bacterial reduction and disproportionation of thiosulfate and sulfite. *Geochim. Cosmochim. Acta* **1998**, *62*, 2585–2595.
53. Makhnach, A.; Mikhajlov, N.; Kolosov, I.; Gulis, L.; Shimanovich, V.; Demeneva, O. Comparative analysis of sulfur isotope behavior in the basins with evaporites of chloride and sulfate types. *Sediment. Geol.* **2000**, *134*, 343–360.
54. Cortecci, G.; Reyes, E.; Berti, G.; Casati, P. Sulfur and oxygen isotopes in Italian marine sulfates of Permian and Triassic ages. *Chem. Geol.* **1981**, *34*, 65–79.
55. Huang, J.; Liu, S. Sulfur isotope distribution of Triassic evaporite and its geological significance in the Sichuan Basin. *Acta Sedimentol. Sin.* **1989**, *7*, 105–110. (In Chinese with English abstract)
56. Strauss, H. The isotopic composition of sedimentary sulfur through time. *Palaeogeogr. Palaeoclimatol. Palaeoecol.* **1997**, *132*, 97–118.
57. Newton, R.J.; Pevitt, E.L.; Wignall, P.B.; Bottrell, S.H. Large shifts in the isotopic composition of seawater sulphate across the Permo–Triassic boundary in northern Italy. *Earth Planet. Sci. Lett.* **2004**, *218*, 331–345.

58. Chen, L. Investigation of sulfur isotopic composition and its geological genesis of marine Triassic anhydrite in the Sichuan Basin. *J. Sichuan Univ. Sci. Eng. (Nat. Sci. Ed.)* **2010**, *23*, 238–248. (In Chinese with English abstract)
59. Horacek, M.; Brandner, R.; Richoz, S.; Povoden-Karadeniz, E. Lower Triassic sulphur isotope curve of marine sulphates from the Dolomites, N-Italy. *Palaeogeogr. Palaeoclimatol. Palaeoecol.* **2010**, *290*, 65–70.
60. Song, H.; Tong, J.; Song, H.; Qiu, H.; Zhu, Y. Excursion of sulfur isotope compositions in the Lower Triassic of South Guizhou, China. *J. Earth Sci.* **2010**, *21*, 158–160.
61. Bojar, A.V.; Halas, S.; Bojar, H.P.; Trembaczowski, A. Late Permian to Triassic isotope composition of sulfates in the Eastern Alps: Palaeogeographic implications. *Geol. Mag.* **2016**, *153*, 797–810.
62. Woods, A.D. Paleoceanographic and paleoclimatic context of Early Triassic time. *C. R. Palevol.* **2005**, *4*, 463–472.
63. Stebbins, A.; Algeo, T.J.; Krystyn, L.; Rowe, H.; Brookfield, M.; Williams, J.; Nye, S.W., Jr.; Hannigan, R. Marine sulfur cycle evidence for upwelling and eutrophic stresses during Early Triassic cooling events. *Earth-Sci. Rev.* **2019**, *195*, 68–82.
64. Song, H.; Tong, J.; Algeo, T.J.; Horacek, M.; Qiu, H.; Song, H.; Tian, L.; Chen, Z.Q. Large vertical $\delta^{13}C_{DIC}$ gradients in Early Triassic seas of the South China Craton: Implications for oceanographic changes related to Siberian Traps volcanism. *Glob. Planet. Change* **2013**, *105*, 7–20.
65. Li, H.; Wignall, P.B.; Jiang, H.; Zhang, M.; Wu, X.; Lai, X. A review of carbon isotope excursions, redox changes and marine red beds of the Early Triassic with insights from the Qinling Sea, northwest China. *Earth-Sci. Rev.* **2023**, *247*, 104623.
66. Shang, W.; Zhang, Y.; Li, K.; Xing, E.; Peng, Y.; Gui, B.; Zhao, H.; Jiang, S. Evidence of sulfur isotope about the sedimentary environment of new type of polyhalite potassium ore in the northeast Sichuan Basin. *Carbonates Evaporites* **2021**, *36*, 56.
67. Thode, H.G.; Monster, J. The sulfur isotope abundances in evaporites and in the ancient oceans. In *Chemistry of the Earth's Crust*; Vinogradov, A.P., Ed.; Israel Program for Scientific Translations: Jerusalem, Israel, 1967; pp. 630–641.
68. Mekhtieva, V.L. Sulfur isotopic composition of sediments and brines of modern and ancient Kara-Bogaz-Gol. *Geokhimiya* **1980**, *5*, 745–752.

Disclaimer/Publisher's Note: The statements, opinions and data contained in all publications are solely those of the individual author(s) and contributor(s) and not of MDPI and/or the editor(s). MDPI and/or the editor(s) disclaim responsibility for any injury to people or property resulting from any ideas, methods, instructions or products referred to in the content.